Electronic Supplementary Material (ESI) for Journal of Materials Chemistry A.

Supporting Information

A biocompatible open system Na-doped $IrO_x(OH)_y$ energy storage device with enhanced charge storage properties and long lifetime

Yi-Chieh Hsieh, Chun-Han (Matt) Lai, Kuang-Chih Tso, Shih-Cheng Chou, Grace J. Whang, Christopher S. Choi, Wai-Hong Cheang, Chao-Yi Chu, Jyh-Fu Lee, Po-Chun Chen, San-Yuan Chen, Bruce S. Dunn, Pu-Wei Wu**

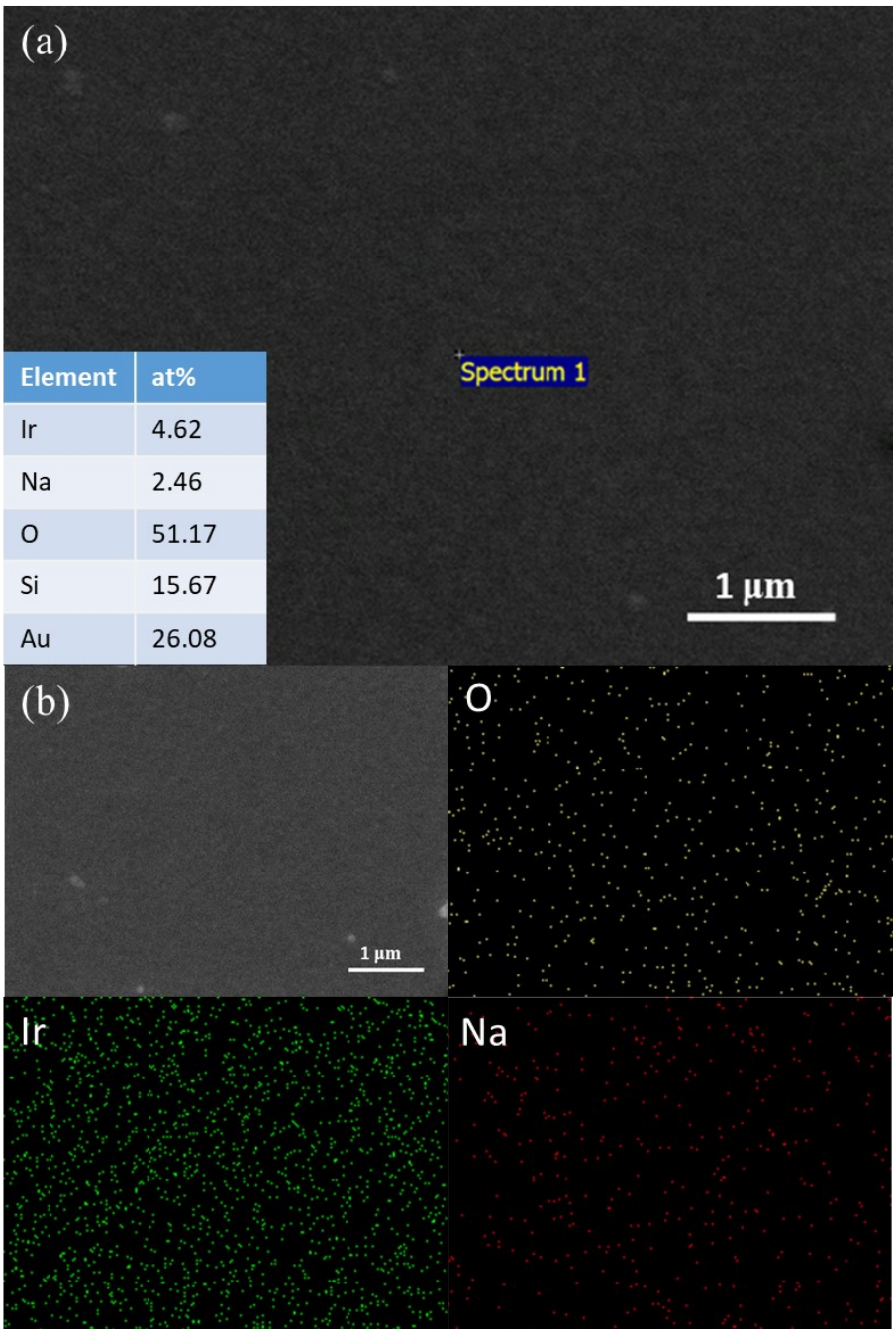

Figure S1. (a) EDX spectra of Na-$IrO_x(OH)_y$ and (b) mapping results corresponding to the selected region from the top-view SEM image.

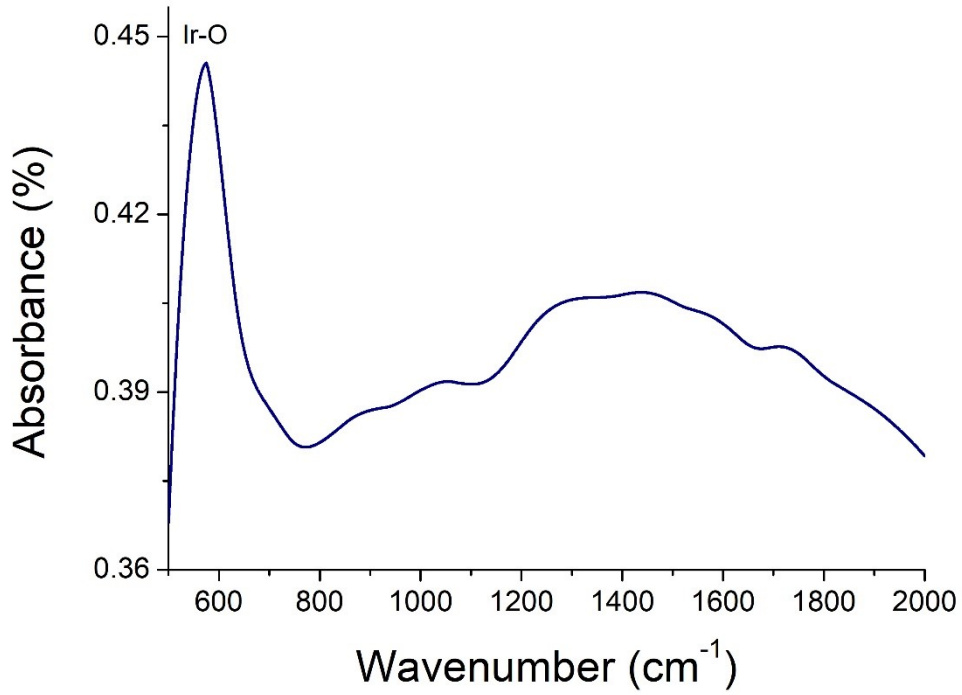

Figure S2. FT-IR analysis of Na-$IrO_x(OH)_y$ after annealing at 550°C for 2 h.

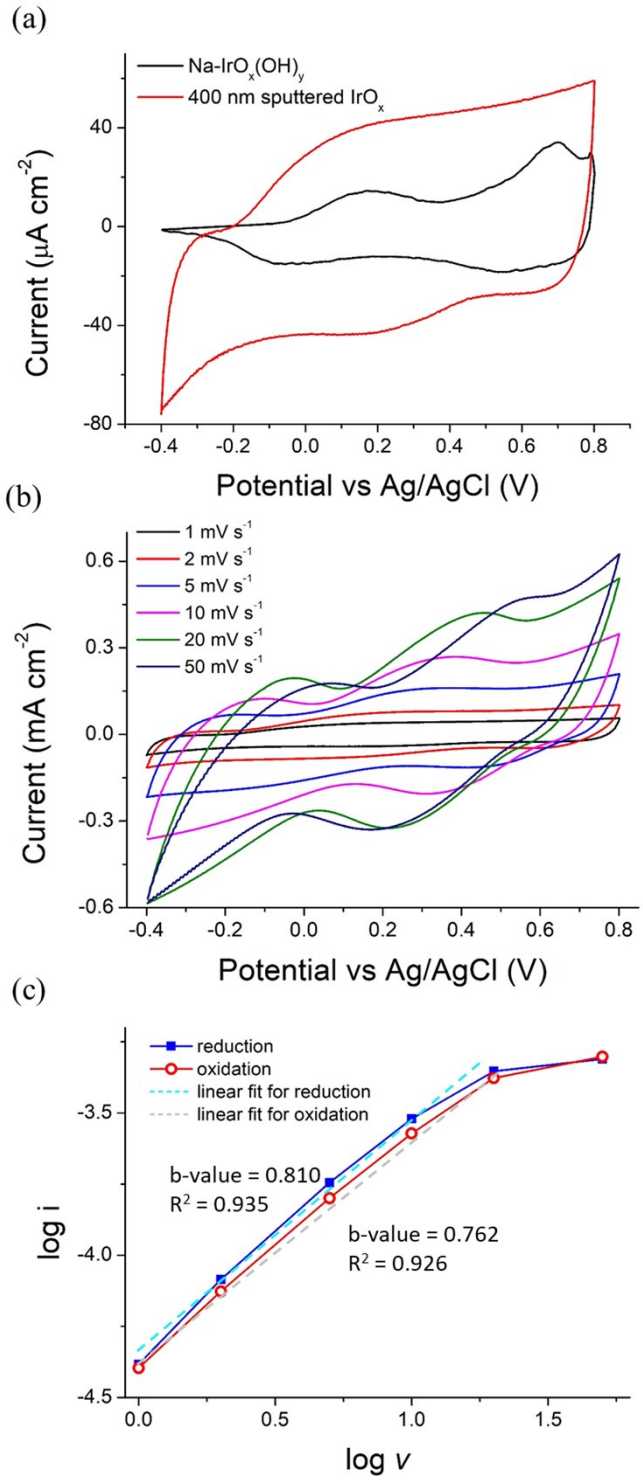

Figure S3. (a) CV profile of Na-$IrO_x(OH)_y$ and 400 nm sputtered IrO_x with a scan rate of 1 mV s^{-1} in PBS. (b) CV profiles of sputtered IrO_x at different scan rates in PBS. (c) The log *v*-log i correlation derived from the reduction and oxidation peaks of sputtered IrO_x.

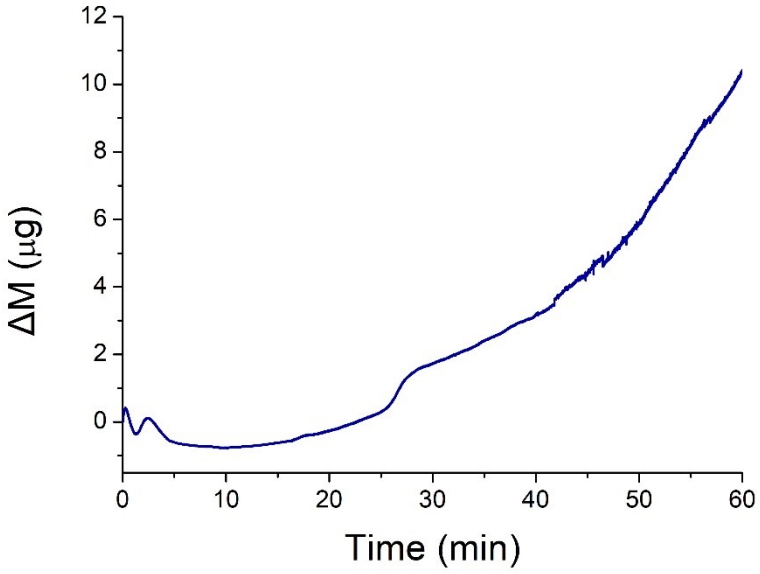

Figure S4. Variation in mass from eQCM during wet chemical deposition of Na-$IrO_x(OH)_y$.

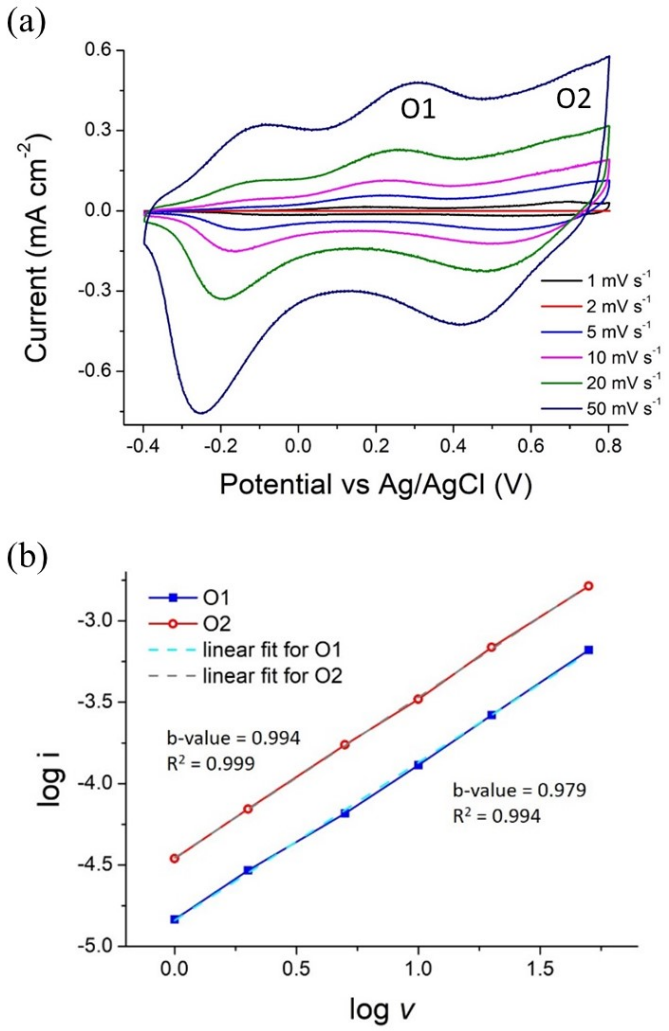

Figure S5. (a) CV profiles of Na-$IrO_x(OH)_y$ at different scan rates in PBS. (b) The log *v*-log i correlation derived from the oxidation peaks as marked as O1 and O2 in Figure 2a.

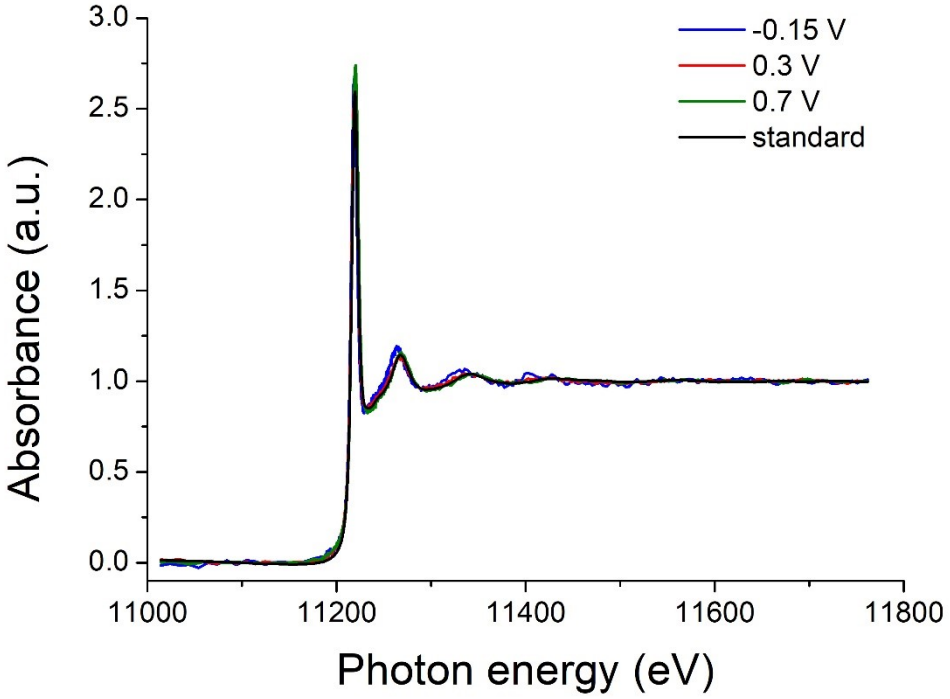

Figure S6. Ir L_{III}-edge spectra of Na-$IrO_x(OH)_y$ held at different potentials and commercial $IrO_2 \cdot H_2O$ powder as the standard.

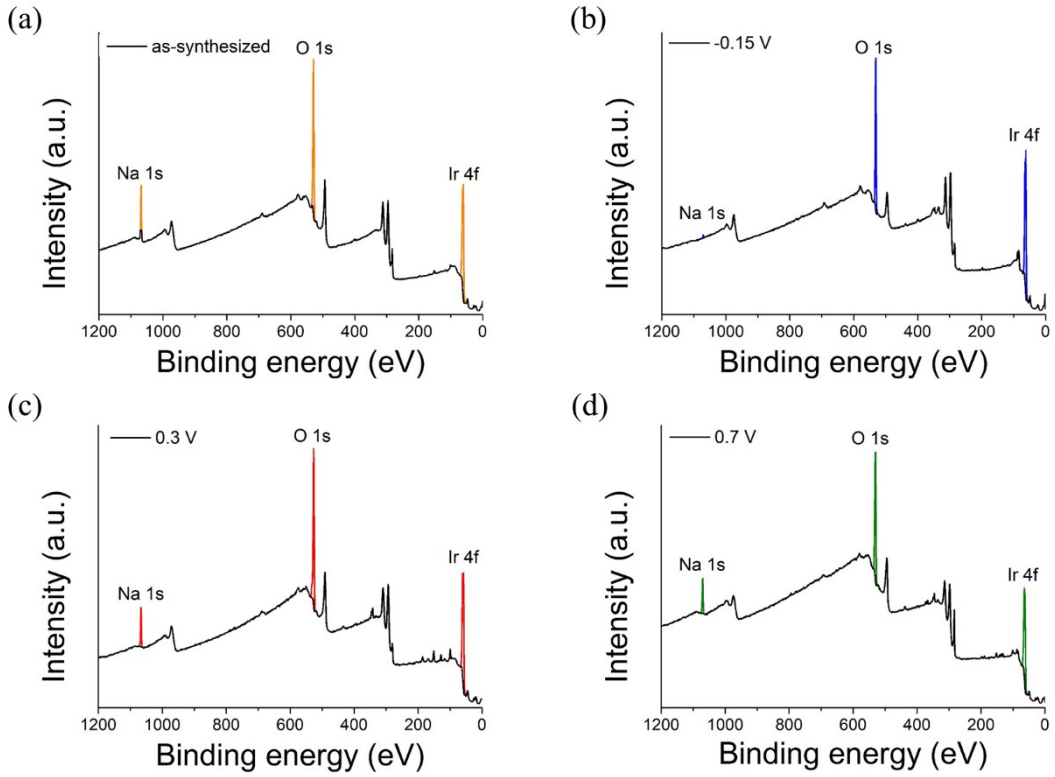

Figure S7. Survey scan of Na-$IrO_x(OH)_y$; (a) as-synthesized as well as at (b) -0.15, (c) 0.3, and (d) 0.7 V.

Table SI. Atomic percentage of Ir, Na, and O derived from the survey scan of Na-$IrO_x(OH)_y$ in Figure S6.

	Ir (at%)	Na (at%)	O (at%)
as-synthesized	15.31	7.22	77.47
-0.15 V	19.97	0.57	79.46
0.3 V	15.14	7.32	77.54
0.7 V	15.00	7.30	77.70

From the fitting results, the chemical composition of the as-synthesized Na-$IrO_x(OH)_y$ sample can be found as $Na_{0.47}IrO_{1.52}(OH)_{1.82}$.

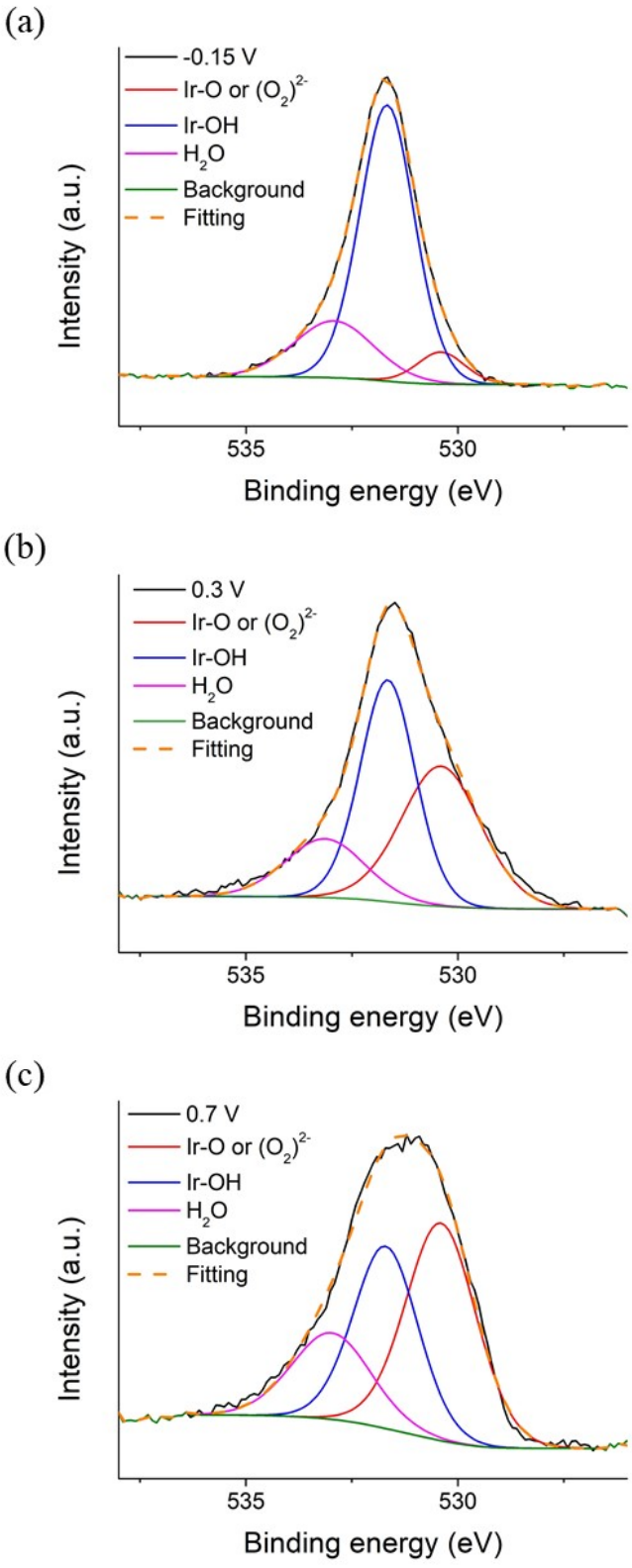

Figure S8. Oxygen stoichiometry determination. The photoemission profile and its fitting curves for O 1s spectrum of Na-$IrO_x(OH)_y$ at (a) -0.15, (b) 0.3, and (c) 0.7 V.

The XAS and XPS results from Figure 3 suggest that the individual redox reactions for proton and sodium occurring in the Na-$IrO_x(OH)_y$ thin film can be written as follows:

$$Ir(III)(OH)_3 \leftrightarrow Ir(IV)O(OH)_2 + H^+ + e^- \quad \text{(S1)}$$

$$Ir(IV)O(OH)_2 \leftrightarrow Ir(V)O_2(OH) + H^+ + e^- \quad \text{(S2)}$$

$$Ir(III)(OH)_3 + xNa^+ \rightarrow Na_xIrO_2O + 3H^+ + (3-x)e^- \quad \text{(S3)}$$

It had been our interest to determine the presence of $(O_2)^{2-}$ from equation (4) at different potentials to obtain full picture of the overall role played by of Na ions. As shown in Figure 3d and S7, we could obtain the O 1s spectrum from different samples. The O 1s spectrum could be fitted by Ir-OH, H_2O, Ir-O, and $(O_2)^{2-}$ peaks.[R1] While the Ir-OH and H_2O peaks could be easily determined, the Ir-O (530.4 eV) and $(O_2)^{2-}$ (530.5 eV) peaks are difficult to be distinguished due to their close proximity. The decrease of Ir-O and $(O_2)^{2-}$ peaks at -0.15 V was obvious from Figure S7, however, the composition of $(O_2)^{2-}$ was unable to be obtained. Hence, the exact value for x in equation 4 was not determined.

R1. V. Pfeifer, T. E. Jones, J. J. Velasco Vélez, C. Massué, R. Arrigo, D. Teschner, F. Girgsdies, M. Scherzer, M. T. Greiner, J. Allan, M. Hashagen, G. Weinberg, S. Piccinin, M. Hävecker, A. Knop-Gericke, and R. Schlögl, *Surf. Interface Anal.*, 2016, **48**, 261-273.

R2. D. Foix, M. Sathiya, E. McCalla, J.-M. Tarascon, and D. Gonbeau, *J. Phys. Chem. C*, 2016, **120**, 862-874.

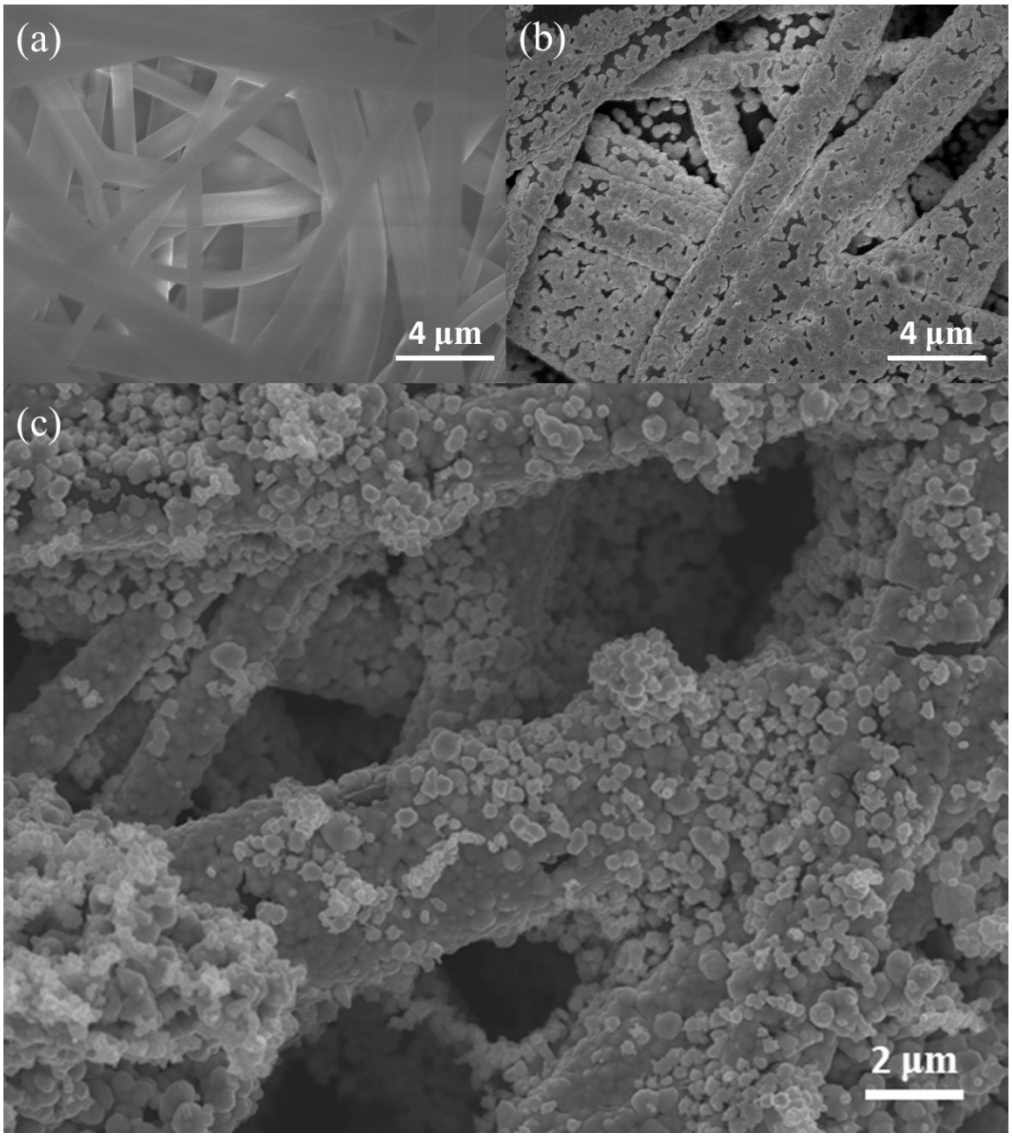

Figure S9. SEM image of (a) PPMM, (b) Au-PPMM, and (c) Na-$IrO_x(OH)_y$-Au-PPMM.

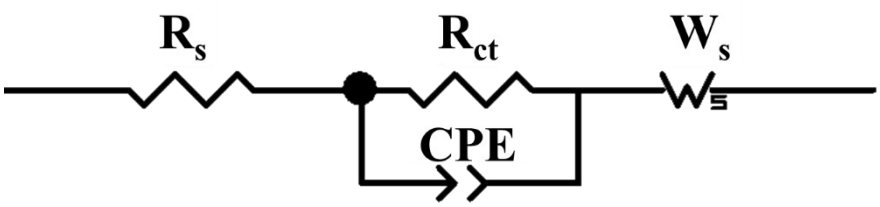

Figure S10. Equivalent circuit model for impedance fitting.

Table SII. Full cell fitting results in L929 solution and PBS.

	R_s (Ω-cm^2)	R_{ct} (Ω-cm^2)
L929 solution	20	4.3
PBS	17	5.2

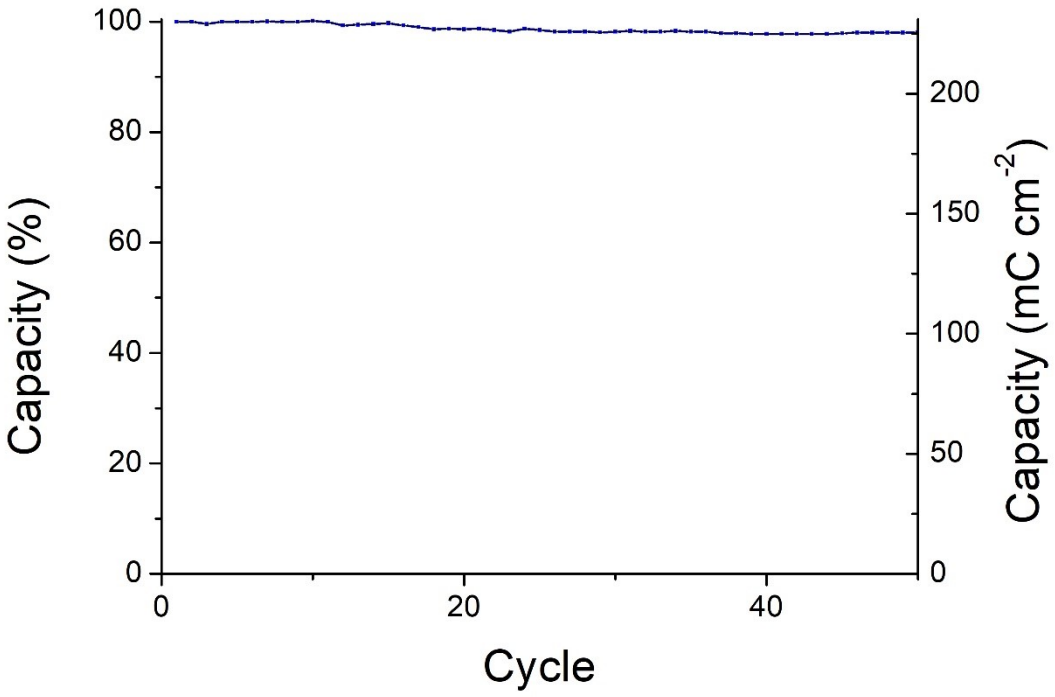

Figure S11. Stability test of Na-$IrO_x(OH)_y$ full cell using GCD at 100 μA cm^{-2} in PBS.

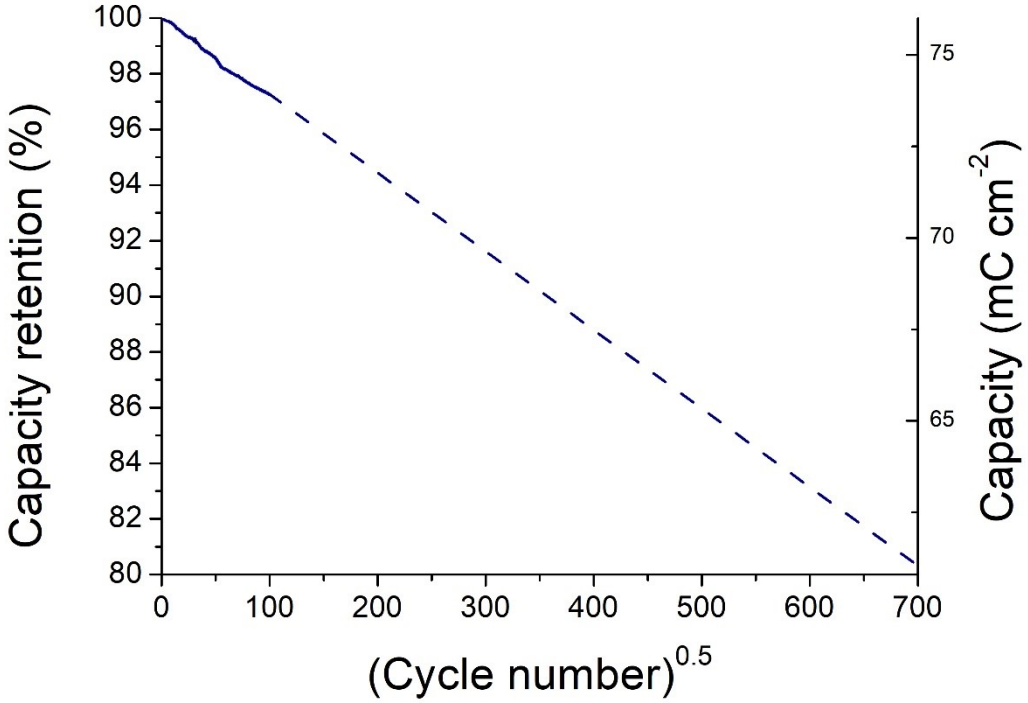

Figure S12. Stability test of Na-$IrO_x(OH)_y$ full cell using CV at 50 mV s^{-1} in PBS.

The capacity retention decreased linearly with increasing square root of the cycle number in the first 10,000 cycle and can be anticipated to reach 80% after near 500k cycles.

Table SIII. Comparisons of different open system supercapacitors in the literature.

Material	Energy density	Power density	Capacity retention	Ref
This work	**6.61 μWh cm^{-2}**	**850 μW cm^{-2}**	**97% / 10,000 cycles**	
ZnO	0.153 μWh cm^{-2}	27 μW cm^{-2}	70% / 1,000 cycles	[39]
PEDOT:PSS/ferr-itin/MWNT fiber	0.82 μWh cm^{-2}	150 μW cm^{-2}	98% / 1,000 cycles	[13]
MnO_2/MWCNT	5 Wh kg^{-1}	3,000 W kg^{-1}	60% / 5,000 cycles	[16]
carbon nanotube fiber	3.18 μWh cm^{-2}	1.04 mW cm^{-2}	98% / 10,000 cycles	[14]
GO and myoblobin	1.1 Wh kg^{-1}	116 W kg^{-1}	98% / 5,000 cycles	[11]
melanin/carbon black	0.122 μWh cm^{-2}	5.24 mW cm^{-2}	61% / 20,000 cycles	[15]

Table SIV. Comparison of total usable energy with implantable energy storage devices in the literature.

	Capacity ($mAh\ cm^{-3}$)	Nominal Voltage (V)	Cycle Life	Usable Energy ($mWh\ cm^{-3}$)	Ref
Close System Devices					
Li primary battery	280	3.3	-	924	[49]
Li-ion thin film battery	200	3.6	1,000	720,000	[50]
primary battery ($Zn\text{-}Ag_2O$)	500	1.6	-	800	[51]
Open System Devices					
biogalvanic cell	270	0.3	-	81	[40]
bio-fuel cell	930	0.32	-	298	[52]
	3	0.5	5,000	7,500	[11]
	1	0.4	1,000	4,000	[13]
supercapacitor	0.45	0.25	10,000	1,125	[R3]
	10	0.4	400	1,600	[R4]
	2.9	0.2	5,000	2,900	[R5]
this work	**2.12**	**0.4**	**10,000**	**8,480**	

The total usable energy was derived by multiplying its energy density by lifetime, which is the number of cycles upon which each device lost 20% of its initial energy, or the highest reported lifetime.

R3. Y. Liu, H. Zhou, W. Zhou, S. Meng, C. Qi, Z. Liu, and T. Kong, *Adv. Energy Mater.*, 2021, **11**, 2101329.

R4. W.-H. Khoh, B.-H. Wee, and J.-D. Hong, *Colloids Surf. A: Physicochem. Eng. Asp.*, 2019, **581**, 123815.

R5. P. Chang, H. Mei, Y. Tan, Y. Zhao, W. Huang, and L. Cheng, *J. Mater. Chem. A*, 2020, **8**, 13646-13658.